Inorg. Chem. **2002**, *41*, 5300−5312

X-ray Diffraction and ^{1}H NMR in Solution: Structural Determination of Lanthanide Complexes of a $Py_2N_6Ac_4$ Ligand

L. Valencia,[†] J. Martinez,[†] A. Macías,[†] R. Bastida,*[,†] R. A. Carvalho,[‡] and C. F. G. C. Geraldes*[,‡]

Departamento de Química Inorgánica, Facultad de Química, Universidad de Santiago de Compostela, Avda. de las Ciencias s/n, E-15782, Santiago de Compostela, Spain, and Departamento de Bioquímica e Centro de Neurociências, Faculdade de Ciências e Tecnologia, Universidade de Coimbra, Apartado 3126, 3001-401 Coimbra, Portugal

Received May 8, 2002

Complexes between the $Py_2N_6Ac_4$ (H_4L) ligand containing four carboxylate pendant arms and trivalent lanthanide ions have been synthesized, and structural studies have been made both in the solid state and aqueous solution. The crystal structures of the La, Ce, Sm, Tb, Dy, Ho, Er, Tm, and Lu complexes, with chemical formulas $[LaH_2L](NO_3)\cdot 3H_2O$ (**1**), $[Ce_4L_2](NO_3)_4\cdot 30H_2O$ (**2**), $[SmHL]\cdot EtOH\cdot 3H_2O$ (**5**), $[TbHL]\cdot EtOH\cdot 3H_2O$ (**8**), $[DyHL]\cdot 2EtOH\cdot 2H_2O$ (**9**), $[HoHL]\cdot 3H_2O$ (**10**), $[ErHL]\cdot EtOH\cdot 3H_2O$ (**11**) $[TmHL]\cdot EtOH\cdot 3H_2O$ (**12**), and $[LuHL]\cdot 3H_2O$ (**14**), have been determined by single-crystal X-ray crystallography. In the solid state, the complexes of the lighter lanthanide ions La^{3+}–Dy^{3+} show a 10-coordinated geometry close to a distorted bicapped antiprism, where the carboxylate pendants are situated alternatively above and below the best plane that contains the nitrogen donor atoms. The complexes of the heavier ions, Ho^{3+}–Lu^{3+}, have a 9-coordinated geometry close to distorted tricapped trigonal prism, with one of the pendant carboxylate groups uncoordinated. The ligand is in a "twist–fold" conformation, where the twisting of the pyridine units is accompanied by an overall folding of the major ring of the macrocycle so that the pyridine nitrogen atoms and the metal are far from linear. The aqueous solution structures of the complexes were thoroughly characterized, the diamagnetic ones (La^{3+} and Lu^{3+}) by their COSY NMR spectra, and the paramagnetic complexes using a linear least-squares fitting of the ^{1}H LIS (lanthanide-induced shift) and LIR (lanthanide-induced relaxation) data with rhombic magnetic susceptibility tensors. The solution structures obtained for the La^{3+}–Dy^{3+} complexes (10-coordinate) and for the Tm^{3+}–Lu^{3+} complexes (9-coordinate) are in very good agreement with the corresponding crystal structures. However, the 10-coordinate structure is still exclusive in solution for the Ho^{3+} complex and predominant for the Er^{3+} complex.

Introduction

Stable, water-soluble complexes between the trivalent lanthanide cations and some polyazamacrocyclic ligands have found a variety of applications, especially in the radiopharmaceutical[1] and biomedical NMR[2,3] fields. The ligands derived from tetraazacyclododecane, CYCLEN, have proven to be particularly useful, because of their high thermodynamic stability and kinetic inertness. The tetraacetate analogue, DOTA, forms the $Gd(DOTA)^-$ chelate, which is one of the most effective and safest magnetic resonance imaging (MRI) contrast enhancement agents available,[4] and the tetramethylenephosphonate analogue, DOTP, forms the $Tm(DOTP)^{5-}$ chelate, which is proving to be a versatile

* Authors to whom correspondence should be addressed. E-mail: geraldes@ci.uc.pt (C.F.G.C.G.). Phone: 351239853608 (C.F.G.C.G.). Fax: 351239853607 (C.F.G.C.G.).

[†] Universidad de Santiago de Compostela.

[‡] Universidade de Coimbra.

(1) (a) Jurisson, S.; Berning, D.; Jia, W.; Ma, D. *Chem. Rev.* **1993**, *93*, 1137. (b) Anderson, C. J.; Welsh, M. J. *Chem. Rev.* **1999**, *99*, 2219. (c) Moi, M. K.; Meares, C. F.; DeNardo, S. J. *J. Am. Chem. Soc.* **1988**, *110*, 6266. (d) Deshpande, S. V.; DeNardo, S. J.; Kukis, D. L.; Moi, M. K.; MaCall, M. J.; DeNardo, G. L.; Meares, C. F. *J. Nucl. Med.* **1990**, *31*, 473.

(2) (a) Sherry, A. D.; Geraldes, C. F. G. C. *Lanthanide Probes in Life, Chemical and Earth Sciencies*; Bünzly, J.-C. G., Chopin, G. R., Eds.; Elsevier: Amsterdam, 1989. (b) Peters, J. A.; Huskens, J.; Raber, D. J. *Prog. Nucl Magn. Reson. Spectrosc.* **1996**, *28*, 283.

(3) (a) Lauffer, R. B. *Chem. Rev.* **1987**, *87*, 901. (b) Caravan, P.; Ellison, J. J.; McMurry, T. J.; Lauffer, R. B. *Chem. Rev.* **1999**, *99*, 2293.

(4) (a) Bousquet, J. C.; Saini, S.; Stark, D. D.; Hahn, P. F.; Niigam, M.; Wittenberg, J.; Ferrucci, J. T. *Radiology* **1988**, *166*, 693. (b) Runge, V. M.; Gelblum, D. Y.; Paccetti, M. L.; Carolan, F.; Heard, G. *Radiology* **190**, *177*, 393.

10.1021/ic0257017 CCC: $22.00
Published on Web 09/13/2002

Chart 1

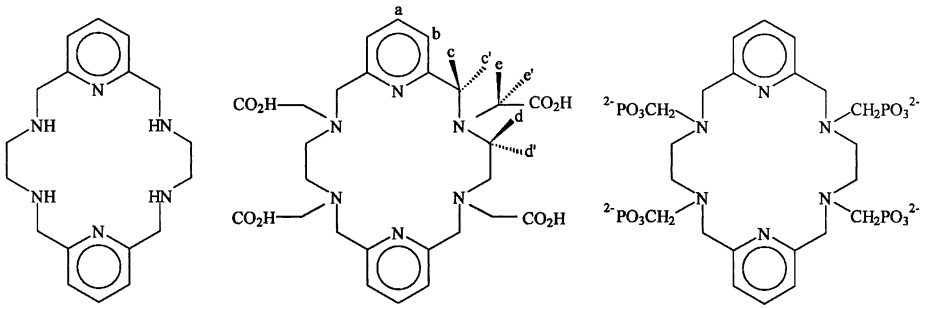

$^{23}Na^+$ NMR shift agent, both for perfused tissues and for in vivo animal studies.[5]

In the search for new macrocyclic derivatives which form stable lanthanide complexes with differing net charges and lipophilicities, studies on some lanthanide complexes containing one or two pyridine moieties as part of their macrocyclic ring have been reported.[6−8] Of particular interest to our study are the chelates containing the 18-membered hexaaza macrocycle $py_2[18]aneN_6$ with four acetate or methylenephosphonate pendant arms.[6a,8b] In this work, we have prepared the hexaaza macrocyclic ligand containing four carboxylate pendant arms, 3,6,14,17,23,24-hexaazatriciclo-[17.3.1.1^{8,12}]tetracosa-1(23),8(24),9,11,19,21-hexaene-3,6,-14,17-tetraacetic acid (**H_4L**, BPO4A or $Py_2N_6Ac_4$, see Chart 1) and report the synthesis of the whole series of its lanthanide(III) complexes. The crystal structures of the La^{3+}, Ce^{3+}, Sm^{3+}, Tb^{3+}, Dy^{3+}, Ho^{3+}, Er^{3+}, Tm^{3+}, and Lu^{3+} complexes were also determined by X-ray diffraction.

The utility of paramagnetic lanthanide(III) complexes as an aid in determining molecular structures and conformation in solution is well established.[2,9] The binding of a ligand to a paramagnetic lanthanide ion induces frequency shifts (landthanide-induced shift, LIS) and relaxation (lanthanide-induced relaxation, LIR) in the NMR spectrum of the ligand relative to that observed for the corresponding diamagnetic complex. The pseudocontact contributions to the observed LIS and LIR can be used to obtain structural information in solution. Thus, the solution structures of the lanthanide(III) complexes have also been studied by NMR spectroscopy, and the solid state and NMR solution structures of these complexes were compared.

Experimental Section

Measurements. Elemental analyses were performed in a Carlo-Erba EA microanalyzer. Infrared (IR) spectra were recorded as KBr disks on a Bruker IFS-66V. FAB mass spectra were recorded using a Kratos-MS-50T spectrometer connected to a DS90 data system using H_2O as the matrix. ^{1}H NMR spectra were recorded on 2 mM solutions of the complexes in D_2O (99.8% D, from Sigma Chem. Co.), with the pD adjusted with DCl or CO_2-free NaOD and converted to pH values using the isotopic correction pH = pD − 0.4, on Bruker DPX 250 (5.8719 T), Bruker AMX 300 (7.0463 T), and Varian Unity 500 (11.7 T) NMR spectrometers, operating at 250.13, 300.13, and 499.80 MHz, respectively. The pD values were measured on a Crison MicropH 2002 pH meter with an Ingold 405-M5 combined electrode (Crison Instruments, Barcelona, Spain). Longitudinal ^{1}H relaxation times (T_1) were measured by the inversion−recovery pulse sequence. Transverse relaxation times (T_2) were measured from the width of the peaks at half-height. The paramagnetic contributions to the relaxation rates were corrected for diamagnetic effects using the T_1 values and the line widths for the La^{3+} complex under the same experimental conditions. ^{1}H NMR spectra of the La^{3+}−Eu^{3+} complexes were assigned using the two-dimensional COSY experiment, which was also used to partially analyze the ^{1}H NMR spectrum of the Lu^{3+} complex.

Analysis of LIS and LIR Data. The LIS and LIR data were analyzed with the aid of the computer programs SHIFT ANALYSIS[9] and LISLIR.[10] In the SHIFT ANALYSIS program,[10] where no assumption is made regarding the magnetic symmetry of the complex,[11] the crystal structures of the complexes were used as input structures, as defined by their Cartesian coordinates with the lanthanide at the origin. The pseudocontact LIS geometric factors were calculated in the molecular coordinate system, and a five-parameter linear least-squares search was used to minimize the

(5) (a) Sherry, A. D.; Geraldes, C. F. G. C.; Cacheris, W. P. *Inorg. Chim. Acta* **1987**, *139*, 137. (b) Sherry, A. D.; Malloy; C. R.; Jeffrey, F. M. H.; Cacheris, W. P.; Geraldes, C. F. G. C. *J. Magn. Reson.* **1988**, *76*, 528. (c) Geraldes, C. F. G. C.; Sherry, A. D.; Kiefer, G. E. *J. Magn. Reson.* **1992**, *97*, 290. (d) Malloy, C. R.; Buster, D. C.; Castro, M. M. C. A.; Geraldes, C. F. G. C.; Jeffrey, F. M. H.; Sherry, A. D. *Magn. Reson. Med.* **1990**, *15*, 33. (e) Bansal, N.; Germann, M. J.; Lazar, I.; Malloy, C. R.; Sherry, A. D. *J. Magn. Reson. Imag.* **1992**, *2*, 385. (f) Bansal, N.; Germann, M. J.; Seshan, V.; Shires, G. T., III; Malloy, C. R.; Sherry, A. D. *Biochemistry* **1993**, *32*, 5638. (g) Seshan, V.; Germann, M. J.; Preisig, P.; Malloy, C. R.; Sherry, A. D.; Bansal, N. *Magn. Reson. Med.* **1995**, *34*, 25.

(6) (a) Kim, W. D.; Hrncir, D. C.; Kiefer, G. E.; Sherry, A. D. *Inorg. Chem.* **1995**, *34*, 2225. (b) Kim, W. D.; Kiefer, G. E.; Maton, F.; McMillan, K.; Muller, R. N.; Sherry, A. D. *Inorg. Chem.* **1995**, *34*, 2243.

(7) (a) Aime, S.; Botta, M.; Crich, S. G.; Giovenzana, G. B.; Jommi, G.; Pagliarin, R.; Sisti, M. *J. Chem. Soc., Chem. Commun.* **1995**, 1885. (b) Aime, S.; Botta, M.; Crich, S. G.; Giovenzana, G. B.; Jommi, G.; Pagliarin, R.; Sisti, M. *Inorg. Chem.* **1997**, *36*, 2992.

(8) (a) Bligh, S. W. A.; Choi, N.; Cummins, W. J.; Evagorou, E. G.; Kelly, J. D.; McPartlin, M. *J. Chem. Soc., Dalton Trans.* **1993**, 3829. (b) Bligh, S. W. A.; Choi, N.; Geraldes, C. F. G. C.; Knoke, S.; McPartlin, M.; Sanganee, M. J.; Woodroffe, T. M. *J. Chem. Soc., Dalton Trans.* **1997**, 4119.

(9) Forsberg, J. H.; Delaney, R. M.; Zhao, Q.; Harakas, G.; Chandran, R. *Inorg. Chem.* **1995**, *34*, 3705.

(10) (a) Peters, J. A.; Peters-van Cranenburgh, P. E. J.; van der Toorn, J. M.; Wortel, T. M.; van Bekkum, H. *Tetrahedron* **1978**, *34*, 2217. (b) Carvalho, R. A.; Peters, J. A.; Geraldes, C. F. G. C. *Inorg. Chim. Acta* **1997**, *262*, 167.

(11) Kemple, M. D.; Ray, B. D.; Lipkowitz, K. B.; Prendergast, F. G.; Rao, B. D. N. *J. Am. Chem. Soc.* **1988**, *110*, 8275.

(12) (a) Willcott, M. R.; Lenkinski, R. E. *J. Am. Chem. Soc.* **1972**, *94*, 1742. (b) Davis, R. E.; Willcott, M. R. *J. Am. Chem. Soc.* **1972**, *94*, 1742.

difference between calculated and observed LIS data. These five parameters were $a_1 = (\chi_{zz} - {}^1/_3\ \mathrm{Tr}\ \chi)$, $a_2 = (\chi_{xx} - \chi_{yy})$, $a_3 = \chi_{xy}$, $a_4 = \chi_{xz}$, and $a_5 = \chi_{yz}$, where χ_{ij} are the main components of the magnetic susceptibility tensor χ and $\mathrm{Tr}\ \chi = \chi_{xx}+\chi_{yy}+\chi_{zz}$. The program also permutes the LIS values over any number of selected nuclei, determining which particular assignment of peaks gives the best fit to the LIS data. The agreement between the observed and the calculated values is evaluated using Hamilton's crystallographic agreement factor (R factor)[12] defined as $R = ([\sum_i (f_{oi} - f_{ci})^2 w_i]/(\sum_i f_{oi}))^{1/2}$, where f_{oi} and f_{ci} are observed and calculated values, respectively, and w_i are weighing factors. Because nonaxial symmetry was found to apply to the complexes studied, the program LISLIR,[9] which assumes axial symmetry for the complexes, was used only in initial computations.

Materials. Pyridine-2,6-dicarbaldehyde was prepared according to literature procedures.[13] Ethyl bromoacetate, ethylenediamine, and lanthanide(III) nitrates were obtained from Aldrich. Solvents used were of reagent grade and purified by usual methods. D_2O (99.8% D), DCl, and NaOD were obtained from Sigma.

Preparation of $Py_2N_6Ac_4$ (H_4L). The synthesis of the ligand **H_4L** was achieved starting from L^1 (py_2[18]aneN_6, see Chart 1), which has involved a template synthesis using Ca(II) as template agent.[14] The synthesis and details of the preparation and X-ray crystal structure of $Py_2N_6Ac_4{\cdot}4HCl{\cdot}4H_2O$ are reported elsewhere.[15,16] $Py_2N_6Ac_4$ was obtained by adding dropwise a solution of ethyl bromoacetate (4.44 mL, 40 mmol) in acetonitrile (50 mL) to a refluxing solution of L^1 (1.63 g, 5 mmol) and Na_2CO_3 (4.24 g, 40 mmol) in acetonitrile (200 mL). The mixture was refluxed for 6 h, allowed to cool, and filtered, and the solution was concentrated to dryness under vacuum. The crude was extracted with Cl_3CH/H_2O, and the combined organic layers were concentrated to dryness. The solid obtained was dissolved in water, and NaOH (1 g, 25 mmol) was added. The solution was refluxed for 4 h, allowed to cool, and stirred at room temperature for 48 h. A 5% solution of HCl was added until the solution reached acidic pH, and the solution was concentrated to dryness to give a crude oil that was dissolved in ethanol and filtered, and the solution was evaporated to dryness to give the ligand $Py_2N_6Ac_4$ (**H_4L**). Yield: 65%. Anal. Calcd for $C_{26}H_{34}N_6O_8$: C, 55.9; H, 6.1; N, 15.1. Found: C, 55.6; H, 6.0; N, 15.3%. FAB mass spectrum: 557 amu. ^{1}H NMR (δ, ppm): $H_{py(p)}$ 7.69 (t, 2H), $H_{py(m)}$ 7.24 (d, 4H), $CH_{2(ax,eq)}$ 3.89 (s, 8H), $CH_{2ac(1,2)}$ 3.59 (s, 8H), $CH_{2en(ax,eq)}$ 2.96 (s, 8H).

Preparation of the Complexes. A solution of $Ln(NO_3)_3{\cdot}xH_2O$ (0.5 mmol) in ethanol (10 mL) was added dropwise to a refluxing solution of $Py_2N_6Ac_4$ (L) (0.281 g, 0.5 mmol) in ethanol (25 mL). The mixture was refluxed for 4 h and allowed to cool. The solution was evaporated to a 5 mL volume, and the precipitate was filtered off yielding the lanthanide complexes of the ligand.

H[LaL](HNO$_3$)·0.9H$_2$O (1). Anal. Calcd for $C_{26}H_{50}N_7O_{20}La$: C, 34.0; H, 5.2; N, 10.7. Found: C, 33.6; H, 4.8; N, 11.3%. Yield: 80%. FAB mass spectrum (negative ion): 693 amu. Crystals of formula $[LaH_2L](NO_3){\cdot}3H_2O$ suitable for X-ray diffraction were grown from an aqueous solution of the isolated solid.

Ce[CeL](NO$_3$)$_2$·5H$_2$O (2). Anal. Calcd for $C_{26}H_{40}N_8O_{19}Ce_2$: C, 31.9; H, 3.3; N, 11.5. Found: C, 29.8; H, 3.8; N, 10.7%. Yield: 82%. FAB mass spectrum (negative ion): 694 amu. Crystals of formula $[Ce_4L_2(H_2O)_{11}](NO_3)_4{\cdot}30H_2O$ suitable for X-ray diffraction were grown from an aqueous solution of the isolated solid.

H[PrL]·5H$_2$O (3). Anal. Calcd for $C_{26}H_{41}N_6O_{13}Pr$: C, 39.7; H, 5.3; N, 10.7. Found: C, 38.8; H, 5.2; N, 11.2%. Yield: 85%. FAB mass spectrum (negative ion): 695 amu.

H[NdL]·8H$_2$O (4). Anal. Calcd for $C_{26}H_{47}N_6O_{16}Nd$: C, 37.0; H, 5.6; N, 10.0. Found: C, 36.5; H, 5.2; N, 10.2%. Yield: 87%. FAB mass spectrum (negative ion): 696 amu.

H[SmL]·5H$_2$O (5). Anal. Calcd for $C_{26}H_{41}N_6O_{13}Sm$: C, 39.2; H, 5.2; N, 10.6. Found: C, 39.1; H, 5.2; N, 11.1%. Yield: 80%. FAB mass spectrum (negative ion): 707 amu. Crystals of formula $[SmHL]{\cdot}EtOH{\cdot}3H_2O$ suitable for X-ray diffraction were grown from an ethanolic solution of the isolated solid.

H[EuL]·6H$_2$O (6). Anal. Calcd for $C_{26}H_{43}N_6O_{14}Eu$: C, 38.2; H, 5.3; N, 10.3. Found: C, 38.3; H, 5.2; N, 10.2%. Yield: 82%. FAB mass spectrum (negative ion): 707 amu.

H[GdL]·5H$_2$O (7). Anal. Calcd for $C_{26}H_{41}N_6O_{13}Gd$: C, 38.9; H, 5.2; N, 10.57. Found: C, 38.4; H, 5.0; N, 11.2%. Yield: 80%. FAB mass spectrum (negative ion): 712 amu.

H[TbL]·6H$_2$O (8). Anal. Calcd for $C_{26}H_{43}N_6O_{14}Tb$: C, 37.9; H, 5.3; N, 10.2. Found: C, 38.3; H, 5.0; N, 10.0%. Yield: 80%. FAB mass spectrum (negative ion): 713 amu. Crystals of formula $[TbHL]{\cdot}EtOH{\cdot}3H_2O$ suitable for X-ray diffraction were grown from an ethanolic solution of the isolated solid.

H[DyL]·3H$_2$O (9). Anal. Calcd for $C_{26}H_{37}N_6O_{11}Dy$: C, 40.3; H, 4.8; N, 10.9. Found: C, 39.9; H, 5.0; N, 11.0%. Yield: 72%. FAB mass spectrum (negative ion): 718 amu. Crystals of formula $[DyHL]{\cdot}2EtOH{\cdot}2H_2O$ suitable for X-ray diffraction were grown from an ethanolic solution of the isolated solid.

[HoHL]·6H$_2$O (10). Anal. Calcd for $C_{26}H_{43}N_6O_{14}Ho$: C, 37.7; H, 5.2; N, 10.1. Found: C, 37.3; H, 5.0; N, 10.2%. Yield: 80%. FAB mass spectrum (negative ion): 719 amu. Crystals of formula $[HoHL]{\cdot}3H_2O$ suitable for X-ray diffraction were grown from an ethanolic solution of the isolated solid.

[ErHL]·5H$_2$O (11). Anal. Calcd for $C_{26}H_{41}N_6O_{13}Er$: C, 38.5; H, 5.1; N, 10.4. Found: C, 38.4; H, 5.0; N, 10.8%. Yield: 73%. FAB mass spectrum (negative ion): 719 amu. Crystals of formula $[ErHL]{\cdot}EtOH{\cdot}3H_2O$ suitable for X-ray diffraction were grown from an ethanolic solution of the isolated solid.

[TmHL]·4H$_2$O (12). Anal. Calcd for $C_{26}H_{39}N_6O_{12}Tm$: C, 39.2; H, 4.9; N, 10.6. Found: C, 38.9; H, 5.0; N, 11.0%. Yield: 80%. FAB mass spectrum (negative ion): 723 amu. Crystals of formula $[TmHL]{\cdot}EtOH{\cdot}3H_2O$ suitable for X-ray diffraction were grown from an ethanolic solution of the isolated solid.

[YbHL]·6H$_2$O (13). Anal. Calcd for $C_{26}H_{43}N_6O_{14}Yb$: C, 37.3; H, 5.2; N, 10.0. Found: C, 37.5; H, 5.2; N, 9.8%. Yield: 75%. FAB mass spectrum (negative ion): 728 amu.

[LuHL]·4H$_2$O (14). Anal. Calcd for $C_{26}H_{39}N_6O_{12}Lu$: C, 38.9; H, 4.9; N, 10.5. Found: C, 38.9; H, 5.0; N, 10.0%. Yield: 70%. FAB mass spectrum (negative ion): 729 amu. Crystals of formula $[LuHL]{\cdot}3H_2O$ suitable for X-ray diffraction were grown from an aqueous solution of the isolated solid.

Crystal Structure Determination for Complexes 5 and 8. Colorless prisms of **5** and **8** were obtained by slow recrystallization of the compound in absolute ethanol and used for the structure determination. The details of the X-ray crystal structure solution and refinement are given in Table 1. Measurements were made on a Enraf-Nonius MACH3 automatic diffractometer. A ψ-scan[17] absorption correction was carried out. The structure of **8** was solved

(13) Alcock, N. W.; Kingston, R. G.; Moore, P.; Pierpoint, C. *J. Chem. Soc., Dalton Trans.* **1984**, 1937.
(14) Rothermel, G. L., Jr.; Miao, L.; Hill, A. L.; Jackels, S. C. *Inorg. Chem.* **1992**, *31*, 4854.
(15) Carvalho, J. F.; Crofts, S. P.; Rocklage, S. M. PCT Patent Application No. WO 91/10645 (EP 91/00126), July 25, 1991.
(16) Kim, W. D. D. Chem. Dissertation, The University of Texas at Dallas, Richardson, TX, 1994.
(17) North, A. C. T.; Phillips, D. C.; Mathews, F. S. *Acta Crystallogr.* **1968**, *A24*, 351.

Table 1. Crystal Data and Structure Refinement for $[LaH_2L](NO_3)\cdot 3H_2O$ (**1**), $[Ce_4L_2(H_2O)_{11}](NO_3)_4\cdot 30H_2O$ (**2**), [SmHL](EtOH)·$3H_2O$ (**5**), [TbHL]EtOH·$3H_2O$ (**8**), [DyHL]·2EtOH·$2H_2O$ (**9**), [HoHL]·$3H_2O$ (**10**), [ErHL]EtOH·$3H_2O$ (**11**), [TmHL]EtOH·$3H_2O$ (**12**), and [LuHL]·$3H_2O$ (**14**)

	1	**2**	**5**	**8**	**9**	**10**	**11**	**12**	**14**
empirical formula	$C_{26}H_{30}N_7O_{15}La$	$C_{52}H_{60}Ce_4N_{16}O_{57}$	$C_{28}H_{28}N_6O_{12}Sm$	$C_{28}H_{30}N_6O_{12}Tb$	$C_{30}H_{35}DyN_6O_{12}$	$C_{26}H_{30}HoN_6O_{11}$	$C_{28}H_{35}ErN_6O_{12}$	$C_{28}H_{30}N_6O_{11}Tm$	$C_{26}H_{30}LuN_6O_{11}$
fw	819.48	2381.64	790.91	801.50	834.14	767.49	814.88	795.51	777.53
T, K	173(2)	173(2)	293(2)	293(2)	173(2)	293(2)	173(2)	173(2)	293(2)
wavelength, Å	0.71073	0.71073	0.71073	0.71073	0.71073	0.71073	0.71073	0.71073	0.71073
cryst syst, space group	monoclinic, $P2(1)/n$	monoclinic, $P2(1)/c$	monoclinic, $P2(1)/n$	monoclinic, $P2(1)/n$	monoclinic, $P2(1)/n$	monoclinic, $C2/c$	orthorhombic, $Pbcn$	orthorhombic, $Pbcn$	monoclinic, $C2/c$
a, Å	9.7586(5)	23.604(3)	10.163(3)	10.1302(14)	10.0692(6)	37.647(5)	11.3079(5)	11.2933(12)	37.528(4)
b, Å	19.5753(10)	19.772(2)	19.329(4)	19.310(4)	19.2742(12)	11.0658(15)	14.3748(7)	14.3595(16)	11.0481(12)
β, deg	92.3040(10)	90.503(2)	97.30(3)	97.401(16)	96.8640(10)	90.103(4)			90.058(4)
c, Å	16.6679(8)	19.185(2)	17.371(5)	17.309(2)	17.1905(11)	14.642(2)	39.5019(19)	39.380(4)	14.6051(15)
V, Å^3	3181.5(3)	8953.1(16)	3384.8(14)	3357.8(9)	3312.3(4)	6099.7(14)	6421.0(5)	6386.1(12)	6055.4(11)
Z, d_{calcd} (Mg/m^3)	4, 1.711	4, 1.767	4, 1.552	4, 1.585	4, 1.673	8, 1.671	8, 1.686	8, 1.655	8, 1.706
abs coeff, mm^{-1}	1.426	2.109	1.802	2.174	2.328	2.661	2.685	2.846	3.328
F(000)	1648	4688	1584	1604	1676	3064	3272	3176	3096
crystal size, mm^3	0.21 × 0.15 × 0.13	0.23 × 0.2 × 0.15	0.24 × 0.16 × 0.08	0.28 × 0.16 × 0.08	0.33 × 0.14 × 0.14	0.28 × 0.27 × 0.25	0.25 × 0.22 × 0.13	0.29 × 0.28 × 0.21	0.60 × 0.56 × 0.47
θ range for data collection, deg	1.61−28.02	1.48−28.04	2.11−30.41	2.11−26.47	1.59−28.01	1.08−30.55	2.06−28.04	2.07−28.03	1.92−33.16
index ranges	$-12 \le h \le 12$, $-25 \le k \le 25$, $-22 \le l \le 10$	$-31 \le h \le 29$, $-25 \le k \le 18$, $-25 \le l \le 20$	$-14 \le h \le 0$, $0 \le k \le 27$, $-24 \le l \le 24$	$-12 \le h \le 0$, $0 \le k \le 24$, $-21 \le l \le 21$	$-13 \le h \le 7$, $-25 \le k \le 23$, $-20 \le l \le 22$	$-53 \le h \le 40$, $-13 \le k \le 15$, $-20 \le l \le 20$	$-14 \le h \le 12$, $-18 \le k \le 11$, $-52 \le l \le 50$	$-11 \le h \le 14$, $-17 \le k \le 18$, $-52 \le l \le 49$	$-57 \le h \le 57$, $-16 \le k \le 14$, $-22 \le l \le 19$
reflns collected/ unique	19193/7389 [R(int) = 0.0464]	52559/20694 [R(int) = 0.0716]	10724/10214 [R(int) = 0.0815]	7317/6920 [R(int) = 0.1410]	20505/7739 [R(int) = 0.0610]	41354/9215 [R(int) = 0.0407]	35938/7637 [R(int) = 0.0559]	35732/7642 [R(int) = 0.1006]	47679/11514 [R(int) = 0.0298]
completeness to 2θ	28.02, 93.6%	28.04, 92.6%	30.41, 97.1%	26.47, 96.7%	28.01, 93.8%	30.55, 47.1%	28.04, 89.2%	28.03, 89.8%	33.16, 47.7%
abs correction	empirical	empirical	ψ-scan	ψ-scan	empirical	empirical	empirical	empirical	empirical
max, min trans	1.00000, 0.79246	1.0000, 0.7424	0.8693, 0.6716	0.8453, 0.5812	1.0000, 0.6598	1.0000, 0.820500	1.0000, 0.6087	1.0000, 0.7089	1.0000, 0.764776
refinement method[a]	*a*	*a*	*a*	*a*	*a*	*a*	*a*	*a*	*a*
data/restraints/ params	7389/0/443	20694/0/1162	10214/0/445	6920/0/413	7739/0/462	9215/0/416	7637/0/425	7642/0/414	11514/0/461
GOF on F^2	0.971	0.914	1.028	0.977	0.986	1.023	1.044	1.225	1.047
final R indices [$I > 2\sigma(I)$]	R1 = 0.0323, wR2 = 0.078	R1 = 0.0474, wR2 = 0.0903	R1 = 0.0612, wR2 = 0.1756	R1 = 0.0725, wR2 = 0.1858	R1 = 0.0486, wR2 = 0.1226	R1 = 0.0300, wR2 = 0.0709	R1 = 0.0441, wR2 = 0.0910	R1 = 0.1169, wR2 = 0.2210	R1 = 0.0258, wR2 = 0.0646
R indices (all data)	R1 = 0.0489, wR2 = 0.0829	R1 = 0.0964, wR2 = 0.1003	R1 = 0.2141, wR2 = 0.2184	R1 = 0.2468, wR2 = 0.2398	R1 = 0.0790, wR2 = 0.1321	R1 = 0.0664, wR2 = 0.0909	R1 = 0.0817, wR2 = 0.1003	R1 = 0.1881, wR2 = 0.2424	R1 = 0.0438, wR2 = 0.0743
extinction coeff			0.0009(2)						
largest diff peak, hole, e·Å^{-3}	1.045, −0.671	1.939, −0.960	3.528, −1.761	2.266, −2.226	1.605, −2.560	1.222, −1.013	0.768, −2.276	2.221, −9.155	1.213, −1.248

[a] Full-matrix least-squares on F^2.

Table 2. Bond Lengths (in Å) of the Metal Coordination Spheres in Complexes **1**, **2**, **5**, **8**, **9**, **10**, **11**, **12**, and **14**

bond	$[LaH_2L]^+$ (**1**)	Ce_1[a] (**2**)	[SmHL] (**5**)	[TbHL] (**8**)	[DyHL] (**9**)	[HoHL] (**10**)	[ErHL] (**11**)	[TmHL] (**12**)	[LuHL] (**14**)
Ln(1)−O(1)	2.571(2)	2.612(4)	2.543(6)	2.543(9)	2.481(4)	2.297(3)	2.282(3)	2.224(10)	2.254(17)
Ln(1)−O(3)	2.572(2)	2.536(4)	2.533(6)	2.463(10)	2.502(4)	2.288(3)	2.282(3)	2.274(13)	2.242(19)
Ln(1)−O(5)	2.550(2)	2.539(4)	2.507(6)	2.478(9)	2.529(4)	*b*	*b*	*b*	*b*
Ln(1)−O(7)	2.723(2)	2.604(4)	2.570(6)	2.504(9)	2.444(4)	2.297(2)	2.294(3)	2.278(11)	2.253(16)
Ln(1)−N(1)	2.637(3)	2.639(4)	2.592(7)	2.597(12)	2.583(5)	2.535(3)	2.511(4)	2.506(13)	2.510(2)
Ln(1)−N(2)	2.698(3)	2.702(5)	2.675(7)	2.627(12)	2.629(5)	2.650(3)	2.644(4)	2.647(14)	2.638(2)
Ln(1)−N(3)	2.701(2)	2.687(5)	2.654(7)	2.629(12)	2.643(5)	2.605(3)	2.600(4)	2.588(12)	2.572(19)
Ln(1)−N(4)	2.636(3)	2.641(5)	2.603(7)	2.572(11)	2.577(5)	2.536(3)	2.524(4)	2.511(11)	2.506(2)
Ln(1)−N(5)	2.692(3)	2.690(5)	2.662(7)	2.619(12)	2.633(5)	2.655(3)	2.627(4)	2.628(12)	2.593(11)
Ln(1)−N(6)	2.718(3)	2.717(5)	2.667(8)	2.654(12)	2.636(6)	2.590(3)	2.586(4)	2.593(11)	2.574(2)
Lu(1)−N(5′)									2.730(2)

[a] Ce^{3+} atom coordinated in the polymer. [b] Oxygen atom not coordinated.

by Patterson methods[18] and subsequent difference Fourier maps, and that of **5** was solved by direct methods which revealed the position of all non-hydrogen atoms. Both structures were refined on F^2 by a full-matrix least-squares procedure using anisotropic displacement parameters for all non-hydrogen atoms.[19] The hydrogen atoms were located in their calculated positions and refined using a riding model.

Crystal Structure Determination for Complexes 1, 2, 9, 10, 11, 12, and 14. A colorless block was obtained by slow recrystallization in D_2O for **1**, and **2**, and in absolute ethanol for **9**, **11**, and **12**, and used for the structure determination. The details of the X-ray crystal structure solution and refinement are given in Table 1. Measurements were made on a Bruker SMART CCD area detector. An empirical absorption correction was carried out. The structures of **2**, **9**, **10**, and **11** were solved by Patterson methods and subsequent difference Fourier maps, and those of **1**, **12**, and **14** were solved by direct methods, which revealed the position of all non-hydrogen atoms. All the structures were refined on F^2 by a full-matrix least-squares procedure using anisotropic displacement parameters for all non-hydrogen atoms. The hydrogen atoms were located in their calculated positions and refined using a riding model. Crystals of **1**, **2**, **9**, **11**, and **12** were unstable at room temperature by losing solvent and were measured at low temperature.

Results and Discussion

The lanthanide complexes of the $Py_2N_6Ac_4$ (L) ligand were synthesized in good yields by reaction of the ligand and the appropriate nitrate metal salt in absolute ethanol. The complexes were characterized by elemental analysis, IR, NMR, and FAB MS. The microanalytical data are consistent with the formulas $H[LaL](HNO_3)\cdot 9H_2O$, $Ce[CeL)](NO_3)_2\cdot 5H_2O$ or $H[LnL]\cdot xH_2O$ (Ln = Pr−Dy, except Pm), and $[LnHL]\cdot xH_2O$ (Ln = Ho−Lu). The negative ion FAB mass spectrum of all the compounds shows a peak assigned to the molecular ion $[LnL]^-$ that confirms the presence of the lanthanide complexes.

X-ray Structures. Crystal Structures of 1, 5, 8, and 9. The structures **5**, **8**, and **9** are isomorphous, and their crystal structures are consistent with the neutral compound [LnHL] (Ln = Sm, Tb, and Dy). Crystal lattices also contain ethanol and water molecules. Although **1** is quite similar to the described complexes, it is not isomorphous with them, having different cell dimensions, and a crystal structure which consists of the cation $[LaH_2L]^+$, a well-separated nitrate anion, and three hydration water molecules. The molecular structure of complex **1** is given in Figure 1A, and selected bond lengths relating to the coordination environment of the metal are given in Table 2 (more complete information including bond angles is listed in Table 1S in the Supporting Information).

The disposition of the donor atoms around the lanthanide ions in complexes **1**, **5**, **8**, and **9** is quite similar (see Figures 1S−5S in the Supporting Information). The metal ion is coordinated within the macrocycle by the six nitrogen donor atoms of the ligand and by four oxygen atoms from the four carboxylate pendant arms, giving rise to a 10-coordinate geometry close to a distorted bicapped antiprism, where the carboxylate pendants are situated alternatively above and below the best plane that contains the nitrogen donor atoms (Figure 2). The structure of the La^{3+} complex with the ligand containing the same 18-membered hexaaza macrocyclic framework and four phosphonate pendant arms, $[La(H_5L^2)]$, has a similar 10-coordinate geometry.[8b] All the crystal structures obtained are centrosymmetric, and both enantiomers (*SSSS*/*RRRR*) are present in the crystal. In the lanthanum complex $[LaH_2L]^+$ (**1**), the distances between the metal ion and the nitrogen donor atoms are slightly shorter (0.1 Å) than in $[La(H_5L^2)]$. As has been observed previously, a progressive decrease of the Ln−donor atom bond distances is observed upon decreasing the ionic radii of the lanthanide ions.[20] In $[LaH_2L]^+$ (**1**), the distance between La^{3+} and the closest pyridinic nitrogen N(4) is 2.636(3) Å, while in [DyHL] (**9**) the Dy−N(4) distance decreases to 2.577(5) Å.

The two types of conformations observed in hexaaza macrocyclic complexes are "twist−wrap", in which the ligand wraps around the metal ion by twisting the pyridyl units relative to each other, and "twist−fold", where the slight twisting of the pyridyl units is accompanied by an overall folding of the macrocyclic ring so that the pyridine nitrogen atoms and the metal are no longer linear.[21] As in the $[La(H_5L^2)]$ structure, the conformation of the macrocyclic framework in all the present structures shows virtually no folding. The angle between the pyridine nitrogen atoms and the lanthanide ion is very similar in all the complexes, the

(18) Sheldrick, G. M. *Acta Crystallogr*. **1990**, *A46*, 467.
(19) Sheldrick, G. M. S*HELXL-97. Program for the Refinement of Crystal Structures*; University of Goettingen: Goettingen, Germany, 1997.
(20) Platas, C.; Avecilla, F.; de Blas, A.; Geraldes, C. F. G. C.; Rodríguez-Blas, T.; Adams, H.; Mahía, J. *Inorg. Chem*. **1999**, *38*, 3190.
(21) Alexander, V. *Chem. Rev*. **1995**, *95*, 273.

average being 179° (173.3° for [La(H_5L^2)]). Nevertheless, the dihedral angle between the pyridine rings is 20.03° in $[LaH_2L]^+$ (**1**) (8.5° for [La(H_5L^2)]), showing that the macrocyclic ligand is slightly twisted. The dihedral angle between the pyridine units in **5**, **8**, and **9** is similar and close to 16°. The lanthanide ion is situated approximately in the best plane through the six macrocycle nitrogen donors (0.03 Å in **1**, 0.003 Å in **5**, 0.005 Å in **8**, and 0.001 Å in **9**). This plane is, however, considerably distorted, with an average rms deviation from planarity of 0.70 Å. The bond lengths in the coordination sphere of **1**, **5**, **8**, and **9** are comparable to the ranges previously observed for 10-coordinated lanthanide complexes.[21]

In the lanthanum complex (**1**), at least one of the four carboxylate pendant groups interacting with the metal must be protonated. The hydrogen may be assigned to the oxygen atom with the longest distance to de carbon [C(26)−O(8) 1.309(4) Å]. In the other 10-coordinated complexes (**5**, **8**, and **9**) where the ligand must be in the $[HL]^{3+}$ form, no C−O bond is significantly longer than the others, and the hydrogen will probably be disordered over the four carboxylate groups.

Crystal Structure of 2. By slow recrystallization of the Ce^{3+} complex in D_2O, crystals suitable for X-ray diffraction were obtained. The structure (Figure 1B) is consistent with a linear polymer formed alternatively by a metal atom endomacrocyclically coordinated by a macrocyclic ligand and an exomacrocyclic metal ion. The asymmetric unit is consistent with four Ce^{3+} atoms and two ligand molecules, where the disposition of the donor atoms around the two endomacrocyclically coordinated metal ions are very similar and equal to the **1**, **5**, **8**, and **9** complexes. They have a 10-coordinate geometry, being coordinated by the six nitrogen donor atoms of the ligand and by four oxygen atoms from the four carboxylate pendant groups, where the carboxylate pendants are situated alternatively above and below the best plane that contains the nitrogen donor atoms. The pyridinic nitrogen atoms provide again the strongest bond to the lanthanide ion (Ce(1)−N(1) 2.639(4) Å, Ce(3)−N(10) 2.627(5) Å). The lanthanide ions are situated approximately in the best plane through the six macrocycle nitrogen donors 0.019 (Ce1) and 0.010 (Ce3), and these planes have an rms of 0.70 and 0.69, respectively. The angles between the pyridinic nitrogen atoms and the Ce ions are very similar to those in the previous structures with a 10-coordinate geometry, complexes **1**, **5**, **8**, and **9** (N(1)−Ce(1)−N(4) 178.44(15)° and N(7)−Ce(3)−N(10) 179.35(16)°), indicating that the structures show virtually no folding. The dihedral angles between the pyridine units are 16° and 13° for the two units, similar to those of **5**, **8**, and **9**.

The coordination shell of the exomacrocyclic metal ion is consistent with eight oxygen atoms; two oxygen atoms of two different carboxylic pendant groups of one adjacent ligand, one oxygen atom of one pendant group from the other adjacent ligand, and five water molecules.

Crystal Structures of 10, 11, 12, and 14. Structures **11** and **12** (see Figure 1C) are isomorphous, as well as **10** and **14**. Selected bond lengths and angles relating to the coordination environment of the metal are given in Table 2 (more complete information including bond angles is listed in Table 1S).

The crystal structures of **10**, **11**, **12**, and **14** (Figures 6S−9S) are different from those of **1**, **2**, **5**, **8**, and **9** and are also consistent with the neutral compound [LnHL] (Ln = Er and Tm). Crystal lattices also contain water molecules and/or ethanol molecules. They have only three of the four carboxylate pendant arms coordinated to the metal ion, as the fourth one extends out away from the metal. The metal ion is then 9-coordinated inside the macrocycle by the six nitrogen donor atoms of the ligand and by three oxygen atoms from three pendant groups, with a coordination geometry close to a distorted tricapped trigonal prism (see Figure 2). The structure can be defined as a "twist−fold" conformation, where the twisting of the pyridine units is accompanied by an overall folding of the major ring of the macrocycle so that the pyridine nitrogen atoms and the metal are far from linear (N(1)−Er−N(4) 148.45(13)° and N(1)−Tm−N(4) 148.9(4)°, N(1)−Ho−N(4) 146.93(10)° and N(1)−Lu−N(4) 146.44(7)°). The dihedral angle between the pyridine units is 51° for **11** and **12**, 60° for **10**, and 61° for **14**. The distance between the metal ion and the closest pyridinic nitrogen is shorter than in the previous structures (N(4)−Ho 2.535(3) Å, N(4)−Er 2.511(4) Å, N(1)−Tm 2.507(12) Å, and N(1)−Lu 2.506(2) Å). The distance of the metal ion to the best plane through the six macrocycle nitrogen donors is 0.2964 Å in **10**, 0.2560 Å in **11**, and 0.2520 Å in **12** (rms 0.7759, 0.78, and 0.7796, respectively). The crystal structure of **14** is disordered, and two positions have been found for the atoms of the free pendant group of the macrocyclic ligand (showing the presence of two conformers in the solid state). The distance of the Lu^{3+} ion to the best plane through the six nitrogen donors is 0.017 and 0.035 Å (for each of the conformers), rms 0.7685 and 0.8212.

Proton NMR Spectra of the Diamagnetic Complexes. ^1H NMR spectra of the La^{3+} and Lu^{3+} complexes were obtained in D_2O solution, at pH 2.0, 4.0, and 6.0. The ^1H NMR spectrum of the lanthanum complex (Figure 3A) did not change with pH, indicating that it can be formulated as $[LaL]^-$ in this pH range, and giving no evidence of protonated complexes, e.g., $[LaHL]^-$. It consists of eight multiplets corresponding to the eight different proton magnetic environments of the ligand molecule (see notation in Chart 1) in only one of the five possible configurations within a 10-coordinate geometry, i.e., the *SSSS* or *RRRR* configuration, where the ligand maintains its 4-fold symmetry upon complex formation in solution,[8b] in accordance with the determined X-ray crystal structure Figure 1A), where all the carboxylate pendant arms are coordinated to the metal ion. The assignments of the proton signals (Table 2S) were based upon shift comparisons with other polyazamacrocyclic polycarboxylate and polyphosphonate lanthanum complexes,[5c,8b,22] and standard 2D homonuclear (COSY) experiments (Figure 10S), which gave strong cross-peaks between the geminal

(22) Aime, S.; Botta, M.; Ermondi, G. *Inorg. Chem.* **1992**, *31*, 4291.

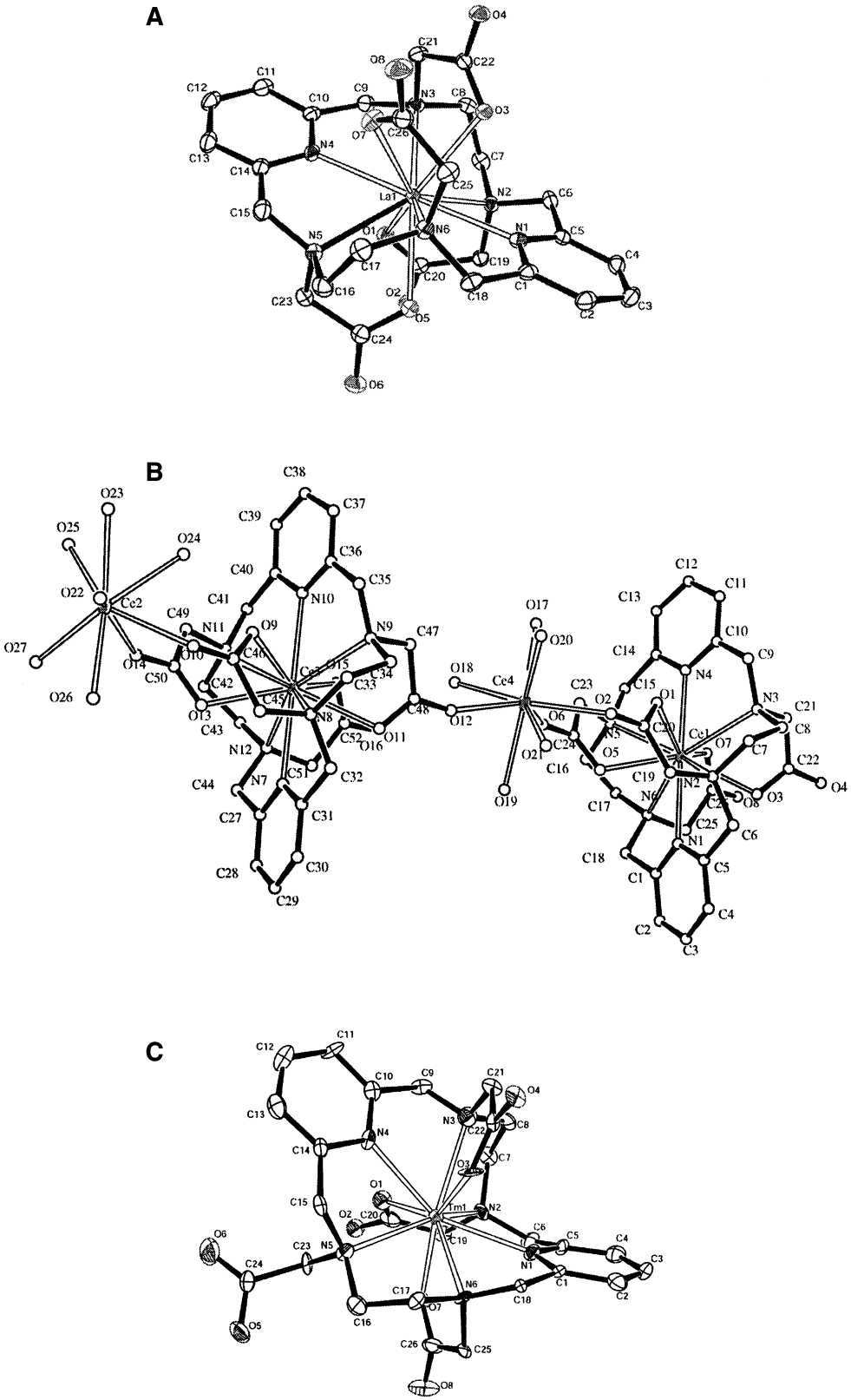

Figure 1. X-ray crystal structures of (A) $[LaH_2L]^+$ (**1**), (B) $[Ce_4L_2]^{4+}$ (**2**), and (C) [TmHL] (**12**) species, showing the atomic numbering scheme. Hydrogen atoms have been omitted for simplicity.

CH_2 protons (c and c′, d and d′, and e and e′) and between the vicinal meta and para pyridyl protons (a and b), and weaker cross-peaks between the meta pyridyl protons (b) and the bridging methylene protons (c and c′) corresponding to four-bond vinyl couplings. Although the specific CH_2 proton assignments $CH_{2en(ax)}/CH_{2en(eq)}$, $CH_{2ac(1)}/CH_{2ac(2)}$, and $CH_{2(ax)}/CH_{2(eq)}$ were not possible on the basis of the 2D NMR spectrum, they were carried out using the stereochemically dependent proton shift effects, resulting from the polarization of the C−H bonds by the electric field effect caused by the

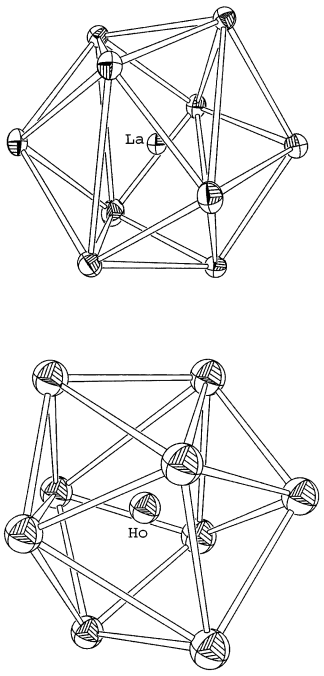

Figure 2. Coordination polyhedra of complexes **1** (top) and **10** (bottom).

cation charge, as well as the ring current shifts induced by the pyridyl rings, as predicted[23] from the X-ray crystal structure of **1**. The spectrum shows a triplet and a doublet, of relative intensities 1:2, centered at δ 7.90 and δ 7.42, corresponding to the pyridyl para $H_{py(p)}$ and meta $H_{py(m)}$ protons, respectively. The bridging methylene protons $CH_{2(ax)}$ and $CH_{2(eq)}$ yield an AB pattern at δ 3.80 and δ 4.49, respectively, where the larger shift for $CH_{2(eq)}$ results from the combined deshielding effects of the pyridyl ring current near the ring plane and polarizing effect of La^{3+} on the $C-H_{eq}$ bond pointing away from it. The methylene carboxylate protons $CH_{2ac(1)}$ and $CH_{2ac(2)}$ also yield an AB pattern at δ 3.19 and δ 3.55, respectively, where the $CH_{2ac(2)}$ methylene protons, those pointing away from the metal ion in the acetate pendant arms, are more deshielded by the electric field effect of La^{3+}. The ethylenic protons $CH_{2en(ax)}$ and $CH_{2en(eq)}$, at the five-membered rings formed by La^{3+} and the ethylenediamine units at the ring N atoms, in rigid $\delta\delta$ or $\lambda\lambda$ configurations, give a AA′XX′ spectrum with two multiplets centered at δ 2.66 and δ 3.19, respectively, where the equatorial protons are more deshielded by the electric field effect of La^{3+}.

While the ^1H NMR spectrum of the Y^{3+} complex is quite similar to that of the La^{3+} complex described previously (data not shown), which indicates that it also has a 10-coordinate geometry, the proton spectrum of the Lu^{3+} complex at pH 2.0 could not be fully assigned because of its complexity (Figure 3C). The large number of signals indicates that the complex adopts an asymmetric structure in solution where the ligand has lost its 4-fold symmetry, in accordance with the presence of an uncoordinated ligand pendant arm in the X-ray crystal structure (see previous description and Figure 1C). This is clearly shown by the presence of two different

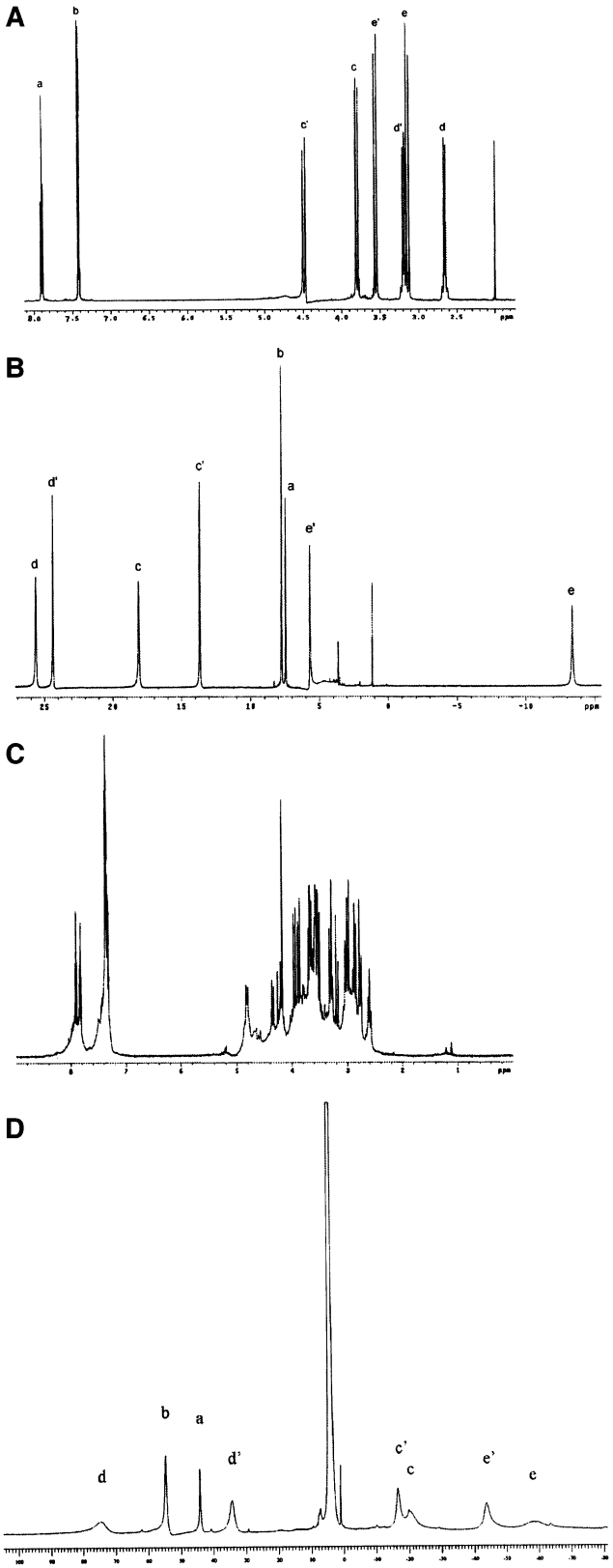

Figure 3. ^1H NMR (500 MHz) spectra of the $[LnL]^-$ complexes in D_2O solution (2 mM, pH = 2.0, 298 K): (A) La^{3+} complex; (B) Pr^{3+} complex; (C) Lu^{3+} complex; (D) Ho^{3+} complex.

triplet signals for the pyridyl para $H_{py(p)}$ protons at δ 7.90 and δ 7.82, which show four COSY cross-peaks (Figure 10S) with the pyridyl meta $H_{py(m)}$ proton doublets at δ 7.36, 7.35, 7.33, and 7.32. In fact, the COSY spectrum shows the same

(23) Harris, R. K. *Nuclear Magnetic Resonance Spectroscopy: A Physicochemical View*; Pitman: London, 1983.

Table 3. ^{1}H NMR Observed LIS Values[a] and Parameters[b] F_i and $G_i = [G_{i1}\langle r^2\rangle A_2^0 + G_{i2}\langle r^2\rangle A_2^2]$[c]

	$CH_{2(ax)}$ (c)	$CH_{2(eq)}$ (c′)	$CH_{2en(ax)}$ (d)	$CH_{2en(eq)}$ (d′)	$CH_{2ac(1)}$ (e)	$CH_{2ac(2)}$ (e′)	$H_{py(m)}$ (b)	$H_{py(p)}$ (a)
				LIS Values				
Ce	9.50	4.80	13.56	10.89	−10.67	−0.97	0.51	0.26
Pr	14.33	9.18	22.99	21.19	−16.53	2.14	0.37	−0.41
Nd	0.16	8.42	11.73	10.53	−9.40	−1.85	6.31	4.76
Sm	0.78	2.24	−1.28	−0.63	1.44	−0.41	0.51	0.35
Eu	−17.43	−11.83	−20.89	−5.75	13.23	−3.47	−3.76	−6.90
Tb	112.80	26.22	145.95	70.85	−120.14	−12.29	3.29	−3.77
Dy	103.20	28.02	141.35	73.81	−100.94	−3.60	2.99	2.50
Ho	−23.60	−20.99	71.45	31.11	−60.14	−46.95	46.99	36.12
Er	−50.80	*d*	−120.65	−82.19	*d*	5.85	47.29	40.60
				Parameters				
F_i	−0.85 ±0.03	−1.21 ±0.02	−1.32 ±0.02	−1.92 ±0.03	0.75 ±0.01	−0.51 ± 0.05	0.41[e] ± 0.01 −0.76[f] ± 0.05 2.52[g] ± 0.01	0.69[e] ± 0.01 −0.80[f] ± 0.01 2.06[g] ± 0.01
G_i	−1.25 ±0.03	−0.57 ±0.02	−1.99 ±0.02	−1.34 ±0.03	1.54 ±0.01	0.15 ±0.05	−0.14[e] ± 0.01 −0.28[f] ± 0.05 0.26[g] ± 0.01	−0.15[e] ± 0.01 −0.25[f] ± 0.01 0.27[g] ± 0.01
R^2	0.910	0.965	0.974	0.933	0.984	0.52	1.00[e] 0.775[f] 1.00[g]	1.00[e] 0.999[f] 1.00[g]

[a] The errors in the measured LIS values are 0.005 ppm for the Ce−Eu complexes and 0.04 ppm for the Tb−Er complexes. [b] The standard deviations of the F_i and G_i parameters are indicated. [c] Resulting from separation plots of the contact and pseudocontact contributions for the paramagnetic $[LnL]^-$ complexes in D_2O based on eq 4 (R^2 values of those correlations are also shown). [d] Not measured. [e] Ce−Pr. [f] Nd−Dy. [g] Ho−Er.

types of cross-peaks observed for the $[LaL]^-$ complex. The bridging methylene protons $CH_{2(eq)}$ and $CH_{2(ax)}$ give four AB patterns, at δ 4.82 and 3.94, δ 4.70 and 3.56, δ 4.59 and 4.35, and δ 4.59 and 3.87 and 3.67, respectively, while the methylene carboxylate protons $CH_{2ac(2)}$ and $CH_{2ac(1)}$ yield three AB patterns at δ 3.67 and 3.56, δ 3.30 and 3.18, and δ 3.00 and 2.75, respectively, for the three bound carboxylates, and one singlet resonance at δ 4.18 for the unbound pendant arm. Because of the asymmetry imposed by the unbound carboxylate, the ethylenic protons $CH_{2en(eq)}$ and $CH_{2en(ax)}$ give two ADMX sets of signals, at δ 3.30, 3.00, 2.87, and 2.60, and at δ 3.60, 3.56, 2.95, and 2.75, respectively, indicating again that the five-membered rings formed by Lu^{3+} with the ethylenediamine units at the ring N atoms adopt rigid $\delta\delta$ or $\lambda\lambda$ configurations. The spectrum of the complex did not change in complexity when the pH was raised to 6.0, showing only small shifts in some of its resonances, presumably because of deprotonation of the unbound pendant acetate arm. Therefore, both the protonated [LuHL] and deprotonated $[LuL]^-$ complexes are asymmetric and 9-coordinated.

Proton NMR Spectra of the Paramagnetic Complexes. ^{1}H NMR spectra of the paramagnetic $[LnL]^-$ complexes (Ln = Ce−Yb, except Pm and Gd) were obtained in D_2O solution (see illustration for $[PrL]^-$ and $[HoL]^-$ in Figure 3B,D, respectively). Each paramagnetic complex (Ce^{3+}−Ho^{3+}) exhibits eight paramagnetically shifted proton resonances corresponding to the same eight groups of protons assigned in the La^{3+} complex, between pH 2.0 and 6.0. The spectra for the Er^{3+}, Tm^{3+}, and Yb^{3+} complexes, like that of the diamagnetic Lu^{3+} complex, are much more complex and could not be fully assigned. A summary of the ^{1}H shifts of the Ce^{3+}−Ho^{3+} complexes at pH 2.0 and 298 K is given in Table 2S. The proton lanthanide-induced shift (LIS) values were measured relative to the corresponding diamagnetic shifts of the La^{3+} complex (Table 3). The ^{1}H NMR spectra of the paramagnetic Ce^{3+}−Eu^{3+} complexes were assigned with the aid of COSY spectra (Figure 10S), which gave cross-peaks between the geminal CH_2 protons and between meta and para pyridyl protons. For these complexes and also for the Dy^{3+}−Ho^{3+} complexes, assignment was aided by plotting the experimental LIS values according to eqs 2 and 3 (see later), allowing for permutations of any two selected nuclei and then determining which particular assignments of peaks gave the best straight lines. Assignments were confirmed by comparison of the experimental and calculated (on the basis of the X-ray crystal structures available) relative proton pseudocontact LIS and the dipolar T_1 LIR values (Pr^{3+} and Nd^{3+} complexes, see later) or the Curie-spin T_2 LIR values obtained from the magnetic field dependence of the signal line widths (Tb^{3+}−Er^{3+} complexes, see later), using the SHIFT ANALYSIS and LISLIR programs. It is worth noting that, while the Ho^{3+} complex still is 10-coordinate in solution, it has a 9-coordinate crystal structure (compound **10**, see Figure 6S and Figure 2).

The ^{1}H NMR spectra of the Er^{3+}, Tm^{3+}, and Yb^{3+} complexes were much more complex (data not shown) and could not be fully assigned. The spectrum of the Er^{3+} complex reveals the presence in solution of a major species of 4-fold symmetry, giving eight signals (some of which could be assigned, see later and Table 2S) corresponding to a 10-coordinate complex, and a minor species with a large number of signals corresponding to a 9-coordinate asymmetric structure, in accordance with the presence of an uncoordinated ligand acetate pendant arm in the X-ray crystal structure of Er^{3+} complex **11** (see above and Figure 7S). The spectra of both the Tm^{3+} and Yb^{3+} complexes consist of about 30 signals each, of about the same intensity and spread between +126.2 and −87.7 ppm, and between +127.4 and −104.5 ppm, respectively, showing that only the 9-coordinate asymmetric structures are present in solution, again in agreement with the presence of an uncoordinated ligand

acetate pendant arm in the X-ray crystal structures of Tm^{3+} complex **12** and Lu^{3+} complex **14** (see previous description and Figures 8S and 9S, respectively).

Separation of Contact and Pseudocontact Shift Contributions. A LIS observed for a nucleus in a Ln^{3+} complex may have contributions from contact and pseudocontact (dipolar) interactions.[2,24,25] If no assumptions are made regarding the location of the principal magnetic axes or the symmetry of the complex, the pseudocontact shift can be expressed by[10,11]

$$\Delta_p = \frac{1}{2N\hbar\gamma_I}(\chi_{zz} - \bar{\chi})\left\langle\frac{3\cos^2-1}{r^3}\right\rangle + \frac{1}{2N\hbar\gamma_I}(\chi_{xx} - \chi_{yy})\left\langle\frac{\sin^2\theta\cos 2\varphi}{r^3}\right\rangle + \frac{1}{N\hbar\gamma_I}\chi_{xy}\left\langle\frac{\sin^2\theta\sin 2\varphi}{r^3}\right\rangle + \frac{1}{N\hbar\gamma_I}\chi_{xz}\left\langle\frac{\sin 2\theta\cos\varphi}{r^3}\right\rangle + \frac{1}{N\hbar\gamma_I}\chi_{yz}\left\langle\frac{\sin 2\theta\sin\varphi}{r^3}\right\rangle \quad (1)$$

where N is Avogadro's $\bar{\chi} = (1/3)\mathrm{Tr}\,\chi$; χ_{xx}, χ_{yy}, χ_{zz}, χ_{xy}, χ_{xz}, and χ_{yz} are the components of the magnetic susceptibility tensor χ in the molecule-fixed ligand system; and r, θ, and φ are the spherical coordinates of the observed nucleus in the coordinate system fixed in the molecule with respect to Ln^{3+} at the origin. The last three terms of eq 1 vanish when the principal magnetic axis is taken as the coordinate system. In the special case of axial symmetry, only the first term remains ($\chi_{xx} = \chi_{yy}$). Pseudocontact shifts have been calculated with the assumption that the ligand field splittings for the lowest J state in the lanthanide complexes are small compared to kT.[25] If the principal magnetic axes system is used, eq 1 can be written as eq 2:

$$\Delta_p = \frac{C_j\beta^2}{60k^2T^2}\left[\frac{\langle r^2\rangle A_2^0(3\cos^2\theta - 1)}{r^3} + \frac{\langle r^2\rangle A_2^2\sin^2\theta\cos 2\varphi}{r^3}\right] \quad (2)$$

where C_j is Bleaney's constant, characteristic of the Ln^{3+} ion, $\langle r^2\rangle A_2^0$ and $\langle r^2\rangle A_2^2$ are ligand field coefficients of the second degree, which are assumed to be constant for an isostructural series of lanthanide complexes.

Thus, the LIS for nucleus i can be expressed as

$$\mathrm{LIS}_i = F_i\langle S_z\rangle_j + C_jG_i \quad (3)$$

where F_i is proportional to the scalar hyperfine coupling constant of the nucleus, $G_i = [G_{i1}\langle r^2\rangle A_2^0 + G_{i2}\langle r^2\rangle A_2^2]$ is a combination of the ligand field coefficients with the geometric factors, $G_{i1} = (3\cos^2\theta - 1)/r^3$ and $G_{i2} = (\sin^2\theta\cos 2\varphi)/r^3$, of the nucleus under observation, and $\langle S_z\rangle_j$ and C_j are, respectively, the spin expectation value and the magnetic constant (Bleaney factor) characteristic of each lanthanide.[24,25]

The pseudocontact and contact contributions to measured LIS values for a series of lanthanide complexes can be separated using a temperature-independent method,[26] which is based on rearrangements of eq 3 into two linear forms:

$$\mathrm{LIS}_i/\langle S_z\rangle_j = F_i + G_i\,C_j/\langle S_z\rangle \quad (4)$$

$$\mathrm{LIS}_i/C_j = F_i\langle S_z\rangle/C_j + G_i \quad (5)$$

For isostructural complexes, plots of $\mathrm{LIS}_i/\langle S_z\rangle_j$ versus $C_j/\langle S_z\rangle_j$ (for largely dipolar LIS values) or of LIS_i/C_j versus $\langle S_z\rangle/C_j$ (for LIS values largely of contact origin) should be linear and yield a unique value for F_i and G_i, as these values are then independent of the lanthanide cation.[26−28]

Plots of the data show that all the protons have both contact and pseudocontact contributions. For the $Ce^{3+}-Ho^{3+}$ complexes, most of the proton LIS data plotted according to eq 4 follow a single linear correlation, with no break observed along that series of lanthanide complexes, indicating that the complexes are isostructural in D_2O solution (see illustration for $H_{ac(1)}$ in Figure 4A). The exceptions are the pyridyl protons, $H_{py(m)}$ (Figure 4B) and $H_{py(p)}$, where the plots show a break between the $Ce^{3+}-Pr^{3+}$ and $Nd^{3+}-Dy^{3+}$ complexes, with a drastic change of the hyperfine coupling constants for these protons but almost no change of G_i. These breaks are then a consequence of the change of A_i and the large contact contribution to the LIS of these protons, located in a delocalized π electron ring system. The values of A_i and G_i determined by linear least-squares analysis of the data obtained are found in Table 3.

Comparison of the Experimental and Calculated Lanthanide Induced Relaxation Rates (LIR). Neglecting the small outer-sphere contribution to the observed LIR values, as well as the small inner-sphere contribution from the contact mechanism, only the dipolar and Curie mechanisms were considered.[2b] Although the dipolar interaction usually dominates the T_1 relaxation of protons, at high magnetic fields the Curie contribution cannot be neglected, even for small complexes of Ln(III) ions (Ln ≠ Gd),[29] in particular in the second half of the series (high μ_{eff}).[30] As both relaxation rate enhancement contributions have the same dependence on the distance r between the nucleus studied and the Ln(III),[2b] their effect can be combined to

$$R_{1p} = 1/T_{1,p} = k/r^6 \quad (6)$$

where the proportionality constant $k = (aT_{1e} + 7bB_0^2\tau_R)$ (for fast rotating small complexes in the extreme narrowing condition, $\omega_H\tau_R \ll 1$) is a function of the electronic spin−lattice relaxation time T_{1e}, the square of the magnetic field B_0, and the rotational correlation time τ_R. At constant

(24) (a) Golding, R. R.; Halton, M. P. *Aust. J. Chem.* **1972**, *25*, 2577. (b) Pinkerton, A. A.; Rossier, M.; Stavros, S. *J. Magn. Reson.* **1985**, *64*, 420.
(25) Bleaney, B. *J. Magn. Reson.* **1972**, *8*, 91.
(26) Reilley, C. N.; Good, B. W.; Allendoerfer, R. D. *Anal. Chem.* **1976**, *48*, 1446.
(27) Reuben, J.; Elgavish, G. *J. Magn. Reson.* **1980**, *39*, 421.
(28) (a) Peters, J. A *J. Magn. Reson.* **1986**, *68*, 240. (b) Ren, J.; Sherry, A. D. *J. Magn. Reson.* **1980**, *39*, 421. (c) Peters, J. A.; Zitha-Bovens, E.; Corsi, D.; Geraldes, C. F. G. C. *The Chemistry of Contrast Agents in Medical Magnetic Resonance Imaging*; Merbach, A. E., Tóth, É., Eds.; Wiley: Chichester, U.K., 2001, Chapter 8, pp 315−381.
(29) Bertini, I.; Capozzi, F.; Luchinat, C.; Nicastro, G.; Xia, Z. *J. Phys. Chem.* **1993**, *97*, 6351.
(30) Aime, S.; Barbero, M.; Botta, M.; Ermondi, G. *J. Chem. Soc., Dalton Trans.* **1992**, 225.

Table 4. Comparison of Relative Ln−Proton Distances *r* Obtained from Experimental LIR Values and Those Calculated from the Crystal Structures

	[PrL]$^-$		[NdL]$^-$		[TbL]$^-$		[DyL]$^-$		[HoL]$^-$
proton	*r*(exptl)[a]	*r*(calcd)[b]	*r*(exptl)[a]	*r*(calcd)[b]	*r*(exptl)[c]	*r*(calcd)[b]	*r*(exptl)[c]	*r*(calcd)[b]	*r*(exptl)[b]
$CH_{2(ax)}$	1.06	1.06	1.13	1.06	1.08	1.08	1.08	1.07	1.13
$CH_{2(eq)}$	1.29	1.25	1.31	1.25	1.26	1.29	1.26	1.26	1.33
$CH_{2en(ax)}$	1.09	1.07	1.27	1.07	1.09	1.08	1.10	1.09	1.12
$CH_{2en(eq)}$	1.30	1.25	1.51	1.25	1.28	1.27	1.28	1.27	1.36
$CH_{2ac(1)}$	1.00	1.00	1.00	1.00	1.00	1.00	1.00	1.00	1.00
$CH_{2ac(2)}$	1.25	1.23	1.27	1.23	1.23	1.18	1.24	1.27	1.25
$H_{py(m)}$	1.57	1.57	1.47	1.57	1.59	1.60	1.60	1.59	1.59
$H_{py(p)}$	1.78	1.80	1.72	1.80	1.83	1.70	1.83	*d*	1.74

[a] Experimental values obtained from the measured T_1 values. [b] Calculated values from the crystal coordinates (for $Pr^{3+}$and Nd^{3+} complexes, the values were obtained with the crystal structure of the La^{3+} complex). [c] Experimental values obtained from the measured magnetic field dependence of the line widths. [d] Not obtained.

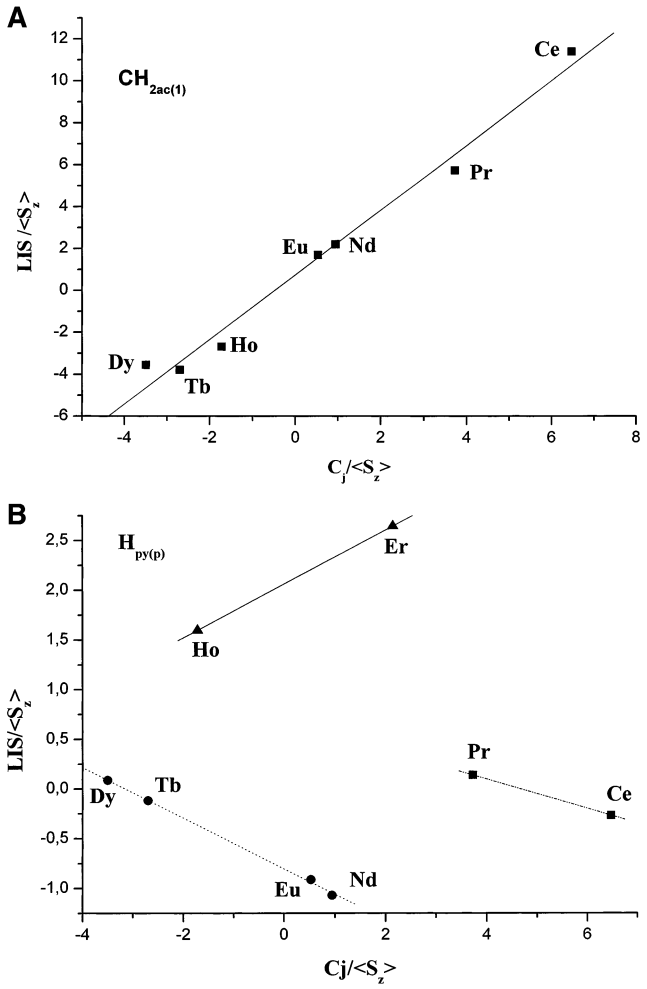

Figure 4. Plot for the separation of contact and pseudocontact contributions to the proton LIS data of the complexes of Ce^{3+}−Ho^{3+} according to eq 4: (A) $H_{ac(1)}$ proton; (B) $H_{py(p)}$.

temperature and B_0, application of eq 6 allows the determination of relative *r* values in the complexes without the need to estimate T_{1e} and τ_R for the complexes, which would be needed to calculate absolute distances. The proton T_1 values were determined for the Pr^{3+} and Nd^{3+} complexes ($T_{1,M}$) and their R_{1p} values, $R_{1p} = 1/T_{1,p} = (1/T_{1,M} - 1/T_{1,0})$, were obtained after correcting the $1/T_{1,M}$ values for the diamagnetic contribution $1/T_{1,0}$ by subtracting the relaxation rates of the same protons in the La^{3+} complex. The relative distances found for both complexes are quite consistent with the relative distances found for the crystal structures of the La^{3+}

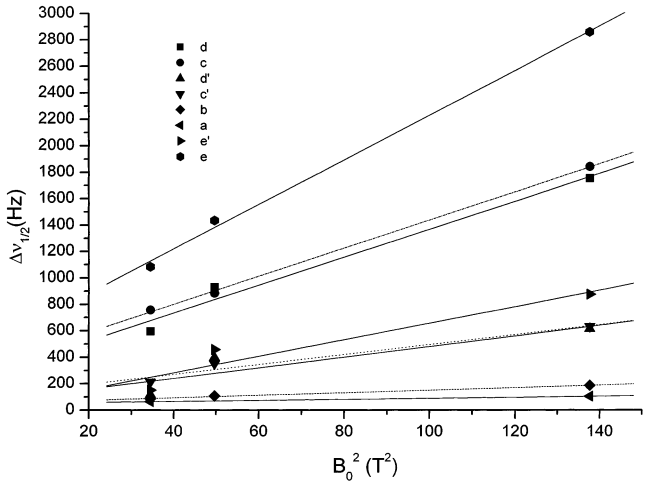

Figure 5. Plot of dependence of line widths $\Delta\nu_{1/2}$ of proton signals (see assignments in Chart 1) on the square of the magnetic field B_0^2 for the complex [TbL]$^-$, in D_2O solutions at 2 mM, 298 K, and pH 2.0.

and Sm^{3+} complexes (Table 4), indicating that the structures of the complexes in the first half of the Ln series are very similar in solution and in the solid state.

The Curie contribution dominates transverse relaxation of protons at high magnetic fields in the second half of the series. The effects of dipolar and Curie mechanisms can be combined to[2b,30]

$$\pi\Delta\nu_{1/2} = R_{2M} = 1/T_{2,M} = k'/r^6 \qquad (7)$$

where (for $\omega_H\tau_R \ll 1$) the proportionality constant $k' = (aT_{1e} + 6bB_0^2\tau_R)$. Line widths at half-height, $\Delta\nu_{1/2}$, of the proton peaks of the Tb^{3+}, Dy^{3+}, and Ho^{3+} complexes were measured at three values of the magnetic field B_0. According to eq 7, plots of $\Delta\nu_{1/2}$ versus B_0^2 (see Figure 5 for the Tb^{3+} complex) should give straight lines with relative slopes which are proportional to the ratios of the inverse sixth power of the relevant metal−proton distances. The relative values of *r* obtained experimentally for the Tb^{3+}, Dy^{3+}, and Ho^{3+} complexes are very similar and consistent with the relative distances obtained from the crystal structures of the Tb^{3+} and Dy^{3+} complexes (Table 4). However, the crystal structure of the Ho^{3+} complex is quite different, with an unbound carboxylate pendant arm, giving much larger *r* values for its $CH_{2(1)}$ and $CH_{2(2)}$ protons. Thus, we conclude again that the Ho^{3+} complex has very different structures in the solid state and in aqueous solution.

Comparison of the Experimental and Calculated LIS Values. Table 5 shows the experimental pseudocontact LIS values for the $[LnL]^-$ complexes (Ln = Ce, Pr, Nd, Eu, Tb, Dy, see Table 5), taken as LIS(exp) = $C_j \cdot G_i$ (eq 2) for each complex and proton, where the experimental values of $G_i = [G_{i1}\langle r^2\rangle A_2^0 + G_{i2}\langle r^2\rangle A_2^2]$ were obtained from the corresponding Reilley plots (eqs 4 and 5). This table also compares these values with the corresponding calculated values, LIS(calcd), obtained using the program SHIFT ANALYSIS and the experimental crystal coordinates of the complexes. The LIS data sets of all the Ln^{3+} complexes studied excluded axial magnetic symmetry, as both LISLIR and SHIFT ANALYSIS runs gave unacceptably high agreement factors. Then, the SHIFT ANALYSIS program was used assuming rhombic symmetry and equal weights of all LIS values in the least-squares analysis. When permutations of the assignments of the LIS values were allowed in the program run, with or without using the JOLT method,[10] the best solutions did not alter the initial assignments. Table 5 shows the calculated values of the pseudocontact shifts obtained using as input structures the crystal coordinates obtained for the $[TbL]^-$ complex. These gave a very good agreement with the experimental data, with $R^2 < 0.01557$ in all cases. The pseudocontact shifts were also calculated for the various complexes in solution using the crystal coordinates available for the Ln^{3+} ion with the closest ionic radius: the $[LaL]^-$ crystal coordinates for the shifts of the Ce^{3+} and Pr^{3+} complexes, the $[SmL]^-$ crystal coordinates for the shifts of the Nd^{3+} and Pr^{3+} complexes, and the $[TbL]^-$ and $[DyL]^-$ crystal coordinates for the shifts of the Tb^{3+} and Dy^{3+} complexes, respectively. The best fits obtained were not better than the ones described previously and in Table 5, with $R^2 = 0.10311$ (Ce, Pr), $R^2 = 0.05730$ (Nd, Eu), and $R^2 = 0.01532$ (Tb, Dy).

The starting molecular axis system had the Tb ion at the origin, with the *y* axis along the N(1)−Tb−N(4) line, while the *x* axis was perpendicular to the best plane defined by the six macrocycle nitrogen donor atoms. The χ magnetic susceptibility tensor obtained in this molecule-fixed ligand axis system was rhombic, and was diagonalized in each case, providing a set of Euler angles $\varphi = 98.3 \pm 2.5°$, $\theta = 39.5 \pm 0.9°$, and $\gamma = -95.8 \pm 2.2°$, that relate the principal magnetic axis system (x', y', z') to the molecular coordinate system. These magnetic axes do not pass through any symmetry element of the complexes. The χ tensor diagonal components obtained ($\chi_{x'x'}$, $\chi_{y'y'}$, $\chi_{z'z'}$) were (432.7 ± 14.4, −34.2 ± 17.0, −398.6 ± 13.9) (Ce), (432.7 ± 14.4, −34.2 ± 17.0, −398.6 ± 13.9) (Pr), (300.1 ± 18.5, −30.2 ± 21.1, −270.0 ± 17.9) (Nd), (274.8 ± 9.2, 21.7 ± 10.8, 253.1 ± 8.8) (Eu), (5907.6 ± 197.2, −466.6 ± 231.6, −5441.1 ± 189.8) (Tb), and (6869.3 ± 229.3, −542.5 ± 269.3, −6326.8 ± 220.7) (Dy), in units of VVk/mol. These values define very large χ tensor anisotropies both along the z' axis, ($\chi_{z'z'} - {}^1/_3$ Tr χ), and in the $x'y'$ plane, ($\chi_{x'x'} - \chi_{y'y'}$): (−398.6, 467.0) (Ce), (−695.9, 815.3) (Pr), (−270.0, 330.3) (Nd), (253.1, −296.5) (Eu), (−5441.1, 6374.2) (Tb), and (−6326.8, 7411.8) (Dy), in units of VVk/mol. Similarly to previous results,[9,31] the trends of the relative

Table 5. Comparison of Experimental and Calculated Pseudocontact LIS Values for the Protons of the Paramagnetic $[LnL]^-$ Complexes

		Ce		Pr		Nd		Eu		Tb		Dy	
proton	G_i[a]	LIS (exptl)[b]	LIS (calcd)[c]	LIS (exptl[b]	LIS (calcd)[c]	LIS (exptl)[b]	LIS (calcd)[c]	LIS (exptl)[b]	LIS (calcd)[c]	LIS (exptl)[b]	LIS (calcd)[c]	LIS (exptl)[b]	LIS (calcd)[c]
$CH_{2(ax)}$	−1.25 ± 0.03	7.88 ± 0.19	8.62 ± 0.50	13.75 ± 0.33	15.07 ± 0.82	5.25 ± 0.13	5.72 ± 0.59	−5.00 ± 0.12	−5.48 ± 0.30	107.5 ± 2.6	117.8 ± 6.4	125.0 ± 3.0	130.7 ± 7.5
$CH_{2(eq)}$	−0.57 ± 0.02	3.59 ± 0.13	4.50 ± 0.31	6.27 ± 0.22	7.50 ± 0.53	2.39 ± 0.08	2.67 ± 0.60	−2.28 ± 0.08	−2.86 ± 0.20	49.0 ± 1.7	61.4 ± 4.2	57.0 ± 2.0	71.4 ± 4.9
$CH_{2en(ax)}$	−1.99 ± 0.02	12.54 ± 0.13	12.66 ± 0.64	21.89 ± 0.22	21.18 ± 1.06	8.36 ± 0.08	8.25 ± 0.65	−7.96 ± 0.08	−7.70 ± 0.39	171.1 ± 1.7	165.6 ± 8.3	199.0 ± 2.0	192.5 ± 9.7
$CH_{2en(eq)}$	−1.34 ± 0.03	8.44 ± 0.19	9.14 ± 0.32	14.74 ± 0.33	16.31 ± 0.58	5.63 ± 0.13	6.31 ± 0.44	−5.36 ± 0.12	−5.93 ± 0.21	115.2 ± 2.6	124.8 ± 4.4	134.0 ± 3.0	148.3 ± 5.6
$CH_{2ac(1)}$	1.54 ± 0.01	−9.70 ± 0.06	−8.15 ± 0.67	−16.94 ± 0.11	−14.23 ± 1.17	−6.47 ± 0.08	−5.17 ± 0.80	6.16 ± 0.04	5.17 ± 0.43	−132.4 ± 0.9	−110.3 ± 8.4	−154.0 ± 1.0	−129.3 ± 10.7
$CH_{2ac(2)}$	−0.08 ± 0.05	0.50 ± 0.32	0.43 ± 0.39	0.88 ± 0.55	0.85 ± 0.65	0.34 ± 0.21	0.39 ± 0.50	−0.32 ± 0.20	−0.27 ± 0.25	6.9 ± 4.3	6.7± 5.1	8.0± 5.0	7.8± 5.9
$H_{py(m)}$	−0.14[d] ± 0.01	0.88 ± 0.06	0.31 ± 0.19	1.54 ± 0.11	0.57 ± 0.33	1.18 ± 0.08	0.14 ± 0.23	−1.12 ± 0.04	−0.21 ± 0.12	24.1 ± 0.9	4.5 ± 2.6	28.0 ± 1.0	5.2 ± 3.0
$H_{py(p)}$	−0.15[d] ± 0.01	−0.95 ± 0.06	−0.28 ± 0.14	1.65 ± 0.11	−0.49 ± 0.24	1.05 ± 0.08	−0.25 ± 0.17	−1.00 ± 0.04	0.18 ± 0.09	21.5 ± 0.9	−3.8 ± 1.9	25.0 ± 1.0	−4.5 ± 2.2

[a] Experimental values of $G_i = [G_{i1}\langle r^2\rangle A_2^0 + G_{i2}\langle r^2\rangle A_2^2]$ obtained from Reilley plots (eqs 4 and 5) and their standard deviations. [b] The pseudocontact contributions to the experimental LIS values, LIS(exptl), were taken as the result of the product $C_j \cdot G_i$ for each complex and proton. Their standard deviations were obtained by multiplying the standard deviations of the G_i parameters by C_j. [c] LIS(calcd) values and their standard deviations were calculated using the program SHIFT ANALYSIS and the crystal coordinates obtained for the Tb^{3+} complex. [d] $Ce^{3+}-Pr^{3+}$ complexes.

values of the χ tensor components and anisotropies along the lanthanide series follow the relative Bleaney factors C_j of the various lanthanides,[25] indicating that the crystal field parameters $\langle r^2\rangle A_2^0$ and $\langle r^2\rangle A_2^2$ are constant for these complexes.

Conclusions. A systematic study was carried out for the structure of the Ln^{3+} chelates of the 18-membered hexaaza macrocyclic ligand, $Py_2N_6Ac_4$, containing two pyridine moieties and four acetate pendant arms,[6a] both in the solid state and aqueous solution. In particular, it was possible for the first time to quantitatively compare the structures of the whole series of paramagnetic Ln^{3+} complexes with the series of crystal structures of the same complexes through a linear least-squares fitting of the ^{1}H LIS data with rhombic magnetic susceptibility tensors, using the SHIFT ANALYSIS program.[10] The crystal structures of the Ln = La, Ce, Sm, Tb, Dy, Ho, Er, Tm, and Lu complexes, determined by single-crystal X-ray crystallography, show that in the solid state the complexes of the lighter lanthanide ions $La^{3+}-Dy^{3+}$ have a 10-coordinated distorted bicapped antiprismatic geometry, with the carboxylate pendants situated alternatively above and below the best plane that contains the nitrogen donor atoms. These structures are very close to that found for the complex of La^{3+} with the same 18-membered hexaaza macrocycle containing four methylenephosphonate pendant arms.[8b] The complexes of the heavier ions, $Ho^{3+}-Lu^{3+}$, have a 9-coordinated distorted tricapped trigonal prismatic geometry, with one uncoordinated pendant carboxylate group. The ligand is in a "twist−fold" conformation, where the twisting of the pyridine units and the overall folding of the major ring of the macrocycle places the pyridine nitrogen atoms and the metal in far from a linear arrangement. It was also possible to characterize the aqueous solution structures of the whole series of paramagnetic Ln^{3+} complexes in great detail, using a linear least-squares fitting of the ^{1}H LIS data with rhombic magnetic susceptibility tensors, on the basis of the crystal coordinates obtained and the SHIFT ANALYSIS program.[10] The solution structures obtained for the $La^{3+}-Dy^{3+}$ complexes (10-coordinate) were found to be in very good agreement with the corresponding crystal structures. However, the transition to the 9-coordinate structures, observed at Ho^{3+} in the crystals, fully occurs in solution only for the $Tm^{3+}-Lu^{3+}$ complexes. In fact, the ^{1}H NMR spectra show that the Ho^{3+} complex is still fully 10-coordinate in solution, a structure that is still predominant for the Er^{3+} complex. This example clearly illustrates the structural differences that may occur in the solid state and in solution along a series of Ln^{3+} macrocyclic complexes. The proton spectra of the $La^{3+}-Ho^{3+}$ complexes, with 10-coordinate solution structures, do not reveal any protonation effect on the bound acetate groups between pH 6.0 and 2.0, while the small shifts of some of the proton resonances of the 9-coordinate $Tm^{3+}-Lu^{3+}$ complexes in this pH range reflect protonation of the unbound acetate arm.

Acknowledgment. We thank Xunta de Galicia (PGIDT-01PXI20901PR) for financial support. This work was carried out within a Portuguese-Spanish Integrated Action (E-1/01, HP2000-0038) and the COST D18 program of the E.U.

Supporting Information Available: X-ray crystallographic files, in CIF format; Figures 1S−9S, showing ORTEP views of the X-ray crystal structures of **1**, **2**, **5**, **8**, **9**, **10**, **11**, **12**, and **14**; Figure 10S, showing the 500 MHz proton COSY spectra of the La^{3+}, Pr^{3+}, and Lu^{3+} complexes; Table 1S, showing the dimensions (distances in Å, angles in deg) of the metal coordination spheres in complexes **1**, **2**, **5**, **8**, **9**, **10**, **11**, **12**, and **14**; Table 2S, showing the ^{1}H shifts of the $[LnL]^-$ complexes (Ln = La−Er). This material is available free of charge via the Internet at http://pubs.acs.org.

IC0257017

(31) (a) Horrocks, W. De W., Jr.; Sipe, J. P., III. *Science* **1972**, *177*, 994. (b) Horrocks, W. De W., Jr.; Sipe, J. P., III; Sudnick, D. In *NMR Shift Reagents*; Sievers, R. E. Academic Press: New York, 1973, pp 53−86. (c) Cramer, R. E.; Maynard, R. B. *J. Magn. Reson*. **1978**, *295*, 31.